

Closed-loop adaptive optics system with a single liquid crystal spatial light modulator

Kainan Yao,^{1,2,*} Jianli Wang,¹ Xinyue Liu,¹ and Wei Liu³

¹Changchun Institute of Optics, Fine Mechanics and Physics, Chinese Academy of Sciences, Changchun, Jilin 130033, China

²University of China Academy of Sciences, Beijing 100049, China

³College of Communication Engineering, Jilin University, Changchun 130012, China
[*yaokainan001@126.com](mailto:yaokainan001@126.com)

Abstract: We describe a closed-loop dynamic holographic adaptive optics system. This system can be realized via one liquid crystal spatial light modulator and one CCD camera. The liquid crystal spatial light modulator is used as the wavefront sensor and corrector, as well as imaging element. CCD detects the spots at holographic image plane and at focal plane of imaging channel simultaneously. The basic principle of the system is introduced first, and then the numerical analysis is presented. On this basis, we report a practical implementation of the dynamic holographic adaptive optics system. The results show that a rapid increase of Strehl ratio and improved image quality at focal plane for deliberately introduced aberrations can be achieved, verifying the feasibility of the system.

© 2014 Optical Society of America

OCIS codes: (090.1000) Aberration compensation; (010.1080) Active or adaptive optics; (230.3720) Liquid-crystal devices; (090.1760) Computer holography.

References and links

1. R. K. Tyson, *Principles of Adaptive Optics* (Academic Press, 1998), pp. 1–25.
2. M. A. A. Neil, M. J. Booth, and T. Wilson, “New modal wavefront sensor: a theoretical analysis,” *J. Opt. Soc. Am. A* **17**(6), 1098–1107 (2000).
3. M. A. A. Neil, M. J. Booth, and T. Wilson, “Closed-loop aberration correction by use of a modal Zernike wavefront sensor,” *Opt. Lett.* **25**(15), 1083–1085 (2000).
4. F. Ghebremichael, G. P. Andersen, and K. S. Gurley, “Holography-based wavefront sensing,” *Appl. Opt.* **47**(4), A62–A69 (2008).
5. G. Andersen, L. Dussan, F. Ghebremichael, and K. Chen, “Holographic wavefront sensor,” *Opt. Eng.* **48**(8), 085801 (2009).
6. S. K. Mishra, R. Bhatt, D. Mohan, A. K. Gupta, and A. Sharma, “Differential modal Zernike wavefront sensor employing a computer-generated hologram: a proposal,” *Appl. Opt.* **48**(33), 6458–6465 (2009).
7. R. Bhatt, S. K. Mishra, D. Mohan, and A. K. Gupta, “Direct amplitude detection of Zernike modes by computer-generated holographic wavefront sensor: Modeling and simulation,” *Opt. Lasers Eng.* **46**(6), 428–439 (2008).
8. C. Liu, F. Xi, H. Ma, S. Huang, and Z. Jiang, “Modal wavefront sensor based on binary phase-only multiplexed computer-generated hologram,” *Appl. Opt.* **49**(27), 5117–5124 (2010).
9. S. Dong, T. Haist, W. Osten, T. Ruppel, and O. Sawodny, “Response analysis of holography-based modal wavefront sensor,” *Appl. Opt.* **51**(9), 1318–1327 (2012).
10. S. Dong, T. Haist, and W. Osten, “Hybrid wavefront sensor for the fast detection of wavefront disturbances,” *Appl. Opt.* **51**(25), 6268–6274 (2012).
11. A. D. Corbett, T. D. Wilkinson, J. J. Zhong, and L. Diaz-Santana, “Designing a holographic modal wavefront sensor for the detection of static ocular aberrations,” *J. Opt. Soc. Am. A* **24**(5), 1266–1275 (2007).
12. F. Feng, I. H. White, and T. D. Wilkinson, “Aberration Correction for Free Space Optical Communications Using Rectangular Zernike Modal Wavefront Sensing,” *J. Lightwave Technol.* **32**(6), 1239–1245 (2014).
13. A. Zepp, S. Gladysz, and K. Stein, “Holographic wavefront sensor for fast defocus measurement,” *J. Adv. Opt. Technol.* **2**, 433–437 (2013).
14. G. Andersen, P. Gelsinger-Austin, R. Gaddipati, P. Gaddipati, and F. Ghebremichael, “Fast, compact, autonomous holographic adaptive optics,” *Opt. Express* **22**(8), 9432–9441 (2014).
15. L. Hu, L. Xuan, Y. Liu, Z. Cao, D. Li, and Q. Mu, “Phase-only liquid crystal spatial light modulator for wavefront correction with high precision,” *Opt. Express* **12**(26), 6403–6409 (2004).
16. J. Munch and R. Wuerker, “Holographic technique for correcting aberrations in a telescope,” *Appl. Opt.* **28**(7), 1312–1317 (1989).

17. G. Andersen and R. Knize, "A high resolution, holographically corrected microscope with a Fresnel lens objective at large working distances," *Opt. Express* **2**(13), 546–551 (1998).
 18. R. Martínez-Cuenca, V. Durán, J. Arines, J. Ares, Z. Jaroszewicz, S. Bará, L. Martínez-León, and J. Lancis, "Closed-loop adaptive optics with a single element for wavefront sensing and correction," *Opt. Lett.* **36**(18), 3702–3704 (2011).
 19. J. Arines, V. Durán, Z. Jaroszewicz, J. Ares, E. Tajahuerce, P. Prado, J. Lancis, S. Bará, and V. Climent, "Measurement and compensation of optical aberrations using a single spatial light modulator," *Opt. Express* **15**(23), 15287–15292 (2007).
-

1. Introduction

Adaptive optics is widely applied in optical technology, for example ground-based telescope system, inertial confinement fusion laser system, retinal imaging system and free space optical communication system. Commonly used adaptive optics systems are composed of two separate and well defined units [1].

One is the wavefront sensor, which measures real-time wavefront aberration as a feedback element. In 2000, a modal wavefront sensor was firstly proposed by Neil, et al. [2, 3], and the application possibility of holographic elements in the wavefront sensor was also raised. Ghebremichael, Andersen, Bhatt and Mishra, et al. applied computer-generated holographic elements into modal wavefront sensor and proposed the holographic wavefront sensor (HWFS), where the detection accuracy of single mode aberration can reach $\lambda/50$ [4–7]. Changhai, et al. optimized the multiplexed hologram design to code large numbers of modes [8]. The method to optimize the response curve was proposed by Dong, et al. [9, 10]. The HWFS has been applied in the ocular wavefront aberration detection system and in the free space optical communication system [11–13]. Recently, Andersen et al. reported a compact holographic adaptive optics system, which could measure and correct wavefront aberration in parallel to each actuator of the deformable mirror [14]. Compared with the Shack-Hartmann wavefront sensor, HWFS is insensitive to scintillation and can reduce the calculation amount of wavefront resolving greatly.

The other one is the wavefront corrector, which operates by changing the optical path of light or changing the refractive index of the transmission medium, which is an important part of an adaptive optics system. Currently, wavefront correctors are mainly continuous surface deformable mirror, segmented deformable mirror, membrane deformable mirror, bimorph deformable mirror, micro-electro-mechanical deformable mirror and liquid crystal spatial light modulator (LC-SLM). The LC-SLM is a competitive selection for adaptive optics due to its low cost, reliability, low power consumption, lack of moving mechanical components, and high resolution [15]. Also, holographic wavefront correction (HWFC), which can be displayed on the LC-SLM, is a well-known wavefront correction method [16, 17].

Some researchers try to simplify the architecture of adaptive optics system and multiplex the wavefront sensor and wavefront corrector into a single LC-SLM. Raul and Justo proposed the spatial and temporal multiplexed methods respectively [18, 19]. The approach proposed in [19] is a sequential operation. Compensation patterns and microlens array of Shack-Hartmann wavefront sensor are alternately implemented onto the LC-SLM, so in one step the device is used for wavefront sensing, whereas in the next step it is converted into the compensating unit. The sequential operation suffers from dead times and a correct operation requires the duty time of the device to be significantly shorter than the timescale for changes of aberration [18]. The approach proposed in [18] uses one half LC-SLM as the wavefront corrector and another half LC-SLM as microlens array of Shack-Hartmann wavefront sensor. So the wavefront sensing and correction can be realized simultaneously.

In this paper, we proposed a closed-loop adaptive optics system based on dynamic holograms, which implements wavefront sensing and correction simultaneously with HWFS and HWFC technologies in a single LC-SLM. The whole adaptive optics system can be realized via one LC-SLM and one CCD camera. We call it dynamic holographic adaptive optics system (DHAOS). In this paper, the basic principle of the system is introduced first,

and then the numerical analysis is presented. On this basis, we report the experiment result of DHAOS. Compared with the approach proposed in [18], our present proposal can use full LC-SLM and realize higher spatial resolution. Compared with the setup in [18], DHAOS is more simplified with less components. DHAOS utilizes a single LC-SLM to realize the full capabilities of adaptive optics system with no loss of spatial resolution and temporal response.

2. Theoretical analysis for DHAOS

According to the principle of HWFS, it consists of a method which allows sequential measurement of each Zernike mode with the other method which allows simultaneous measurement of all Zernike modes. DHAOS uses the simultaneous measurement method so that the dynamic wavefront aberration can be measured and compensated. The basic principle of DHAOS is shown as Fig. 1(a). Sub-hologram $2i-1$ is produced through the interference of the Zernike-mode $bZ_i(x, y)$ aberration of light-wave $O_{2i-1}(x, y)$ and a reference spherical wave $R_{2i-1}(x, y)$ converged at point A (x_A, y_A, z_A) . Sub-hologram $2i$ is produced through the interference of the same Zernike-mode $-bZ_i(x, y)$ aberration of light-wave $O_{2i}(x, y)$ and a reference spherical wave $R_{2i}(x, y)$ converged at B point (x_B, y_B, z_B) .

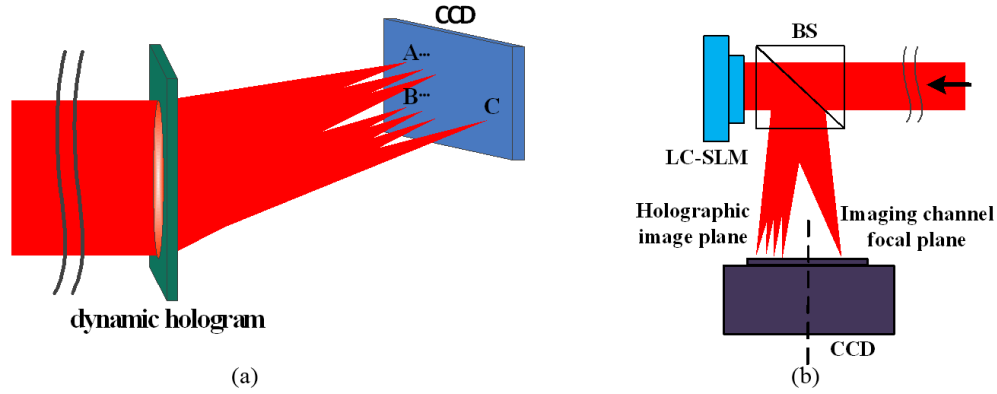


Fig. 1. (a) The schematic diagram of DHAOS and (b) the configuration of DHAOS in numerical simulation.

Light transmittance functions of the two sub-holograms are as follows.

$$\begin{aligned}
 h_{2i-1}(x, y) &= |O_{2i-1}(x, y) + R_{2i-1}(x, y)|^2 \\
 &= O_{2i-1}(x, y)^2 + R_{2i-1}(x, y)^2 \\
 &\quad + O_{2i-1}(x, y)R_{2i-1}^*(x, y) + O_{2i-1}^*(x, y)R_{2i-1}(x, y) \\
 h_{2i}(x, y) &= |O_{2i}(x, y) + R_{2i}(x, y)|^2 \\
 &= O_{2i}(x, y)^2 + R_{2i}(x, y)^2 \\
 &\quad + O_{2i}(x, y)R_{2i}^*(x, y) + O_{2i}^*(x, y)R_{2i}(x, y)
 \end{aligned} \tag{1}$$

With a computer-generated hologram (CGH) rather than an analog hologram recording, we can easily omit the zero-order terms in Eq. (1) to increase the diffraction efficiency. Light transmittance functions of the two CGHs are as follows.

$$\begin{aligned}
H_{2i-1}(x, y) &= O_{2i-1}^*(x, y)R_{2i-1}(x, y) \\
&= \exp\{-jbZ_i(x, y)\} \times \exp\{-jk[(x-x_A)^2 + (y-y_A)^2 + z_A^2]^{1/2}\} \\
H_{2i}(x, y) &= O_{2i}^*(x, y)R_{2i}(x, y) \\
&= \exp\{jbZ_i(x, y)\} \times \exp\{-jk[(x-x_B)^2 + (y-y_B)^2 + z_B^2]^{1/2}\}
\end{aligned} \tag{2}$$

Due to the properties of holographic element, the two sub-holograms are superimposed to form a multiplexed hologram that contains the Zernike-mode aberration information. When a light-wave of $W(x, y)$ with the same mode aberration illuminates the hologram, two spherical waves modulated by aberration will emerge concurrently, and converge at points A and B respectively.

$$\begin{aligned}
H_{2i-1}(x, y) \times W(x, y) &= \exp\{ja_i Z_i(x, y) + j \sum_{\substack{m=1 \\ m \neq i}}^n a_m Z_m(x, y)\} \times \exp\{-jbZ_i(x, y)\} \\
&\quad \times \exp\{-jk[(x-x_A)^2 + (y-y_A)^2 + z_A^2]^{1/2}\} \\
H_{2i}(x, y) \times W(x, y) &= \exp\{ja_i Z_i(x, y) + j \sum_{\substack{m=1 \\ m \neq i}}^n a_m Z_m(x, y)\} \times \exp\{jbZ_i(x, y)\} \\
&\quad \times \exp\{-jk[(x-x_B)^2 + (y-y_B)^2 + z_B^2]^{1/2}\}
\end{aligned} \tag{3}$$

According to the principle of HWFS, as $a_i = b$, the peak energy at point B is the weakest. As $a_i = -b$, the peak energy at point A is the weakest. Thus, amplitude of aberration of incident light wave a_i can be obtained by detecting relative light intensity at points A and B. The relative light intensity at points A and B can be written, in the form of first moment, as:

$$P_w = \frac{I_A - I_B}{I_A + I_B} \tag{4}$$

To measure more Zernike-mode aberrations, according to the characteristics of holographic element, more pairs of sub-holograms are superimposed correspondingly and the wave vector directions of relevant spherical waves are controlled to make the focused spots separated spatially. Through the measurement of the relative light intensity of each pair of spots, the corresponding Zernike-mode amplitude can be obtained and the distorted wavefront can be fitted.

We superimposed an imaging hologram, the complex amplitude transmittance of which is shown as Eq. (5), to the above multiplexed hologram. Λ is a coefficient in Eq. (5). The system under the effect of imaging hologram will be imaged at the point C (x_C, y_C, z_C).

$$H_{2n+1}(x, y) = \Lambda \exp\{-jk[(x-x_C)^2 + (y-y_C)^2 + z_C^2]^{1/2}\} \tag{5}$$

After all the above holograms are superimposed and then multiplied by a correction term, the complex amplitude transmittance of multiplexed hologram is got as follows.

$$H(x, y) = \left[\sum_{m=1}^{2n+1} H_m(x, y) \right] \times \exp\left\{j \sum_{i=1}^n -c_i Z_i(x, y)\right\} \tag{6}$$

After the incidence of the light wave $W(x, y)$ with wavefront distortion due to n Zernike-mode aberrations upon the hologram, the light field distribution is as follows.

$$\begin{aligned}
W(x, y) \times H(x, y) &= \exp \left\{ j \sum_{i=1}^n a_i Z_i(x, y) \right\} \\
&\times \left[\sum_{m=1}^{2n+1} H_m(x, y) \right] \times \exp \left\{ j \sum_{i=1}^n -c_i Z_i(x, y) \right\} \\
&= \exp \left\{ j \sum_{i=1}^n (a_i - c_i) Z_i(x, y) \right\} \times \left[\sum_{m=1}^{2n+1} H_m(x, y) \right]
\end{aligned} \quad (7)$$

It can be seen from Eq. (7) that after the correction term is added into the hologram, the hologram has another function called wavefront correction. DHAOS can detect wavefront aberrations via HWFS in real time, and dynamically change the Zernike-mode aberration coefficient c_i of the correction term added in the hologram to implement the closed-loop correction of wavefront aberration. In Eq. (5), the coefficient Λ of imaging hologram can be used to change the ratio of light energy on the spot of imaging hologram to that on the spots of the other holograms, according to the characteristics of multiplexed hologram.

3. Numerical simulation of DHAOS

We carried out numerical simulation upon DHAOS, the configuration of which is shown in Fig. 1(b). Simulation parameters are selected as follows. The sampling points of the hologram, which is displayed by the LC-SLM, are 512×512 . The laser wavelength is 632.8nm. The aperture of the hologram is 6mm. The distance between the detection plane and the hologram is 3000mm. The distance between focal spot and the axis is greater than 1cm, and the low 12 Zernike-mode aberrations are detected, that are $Z(2, 0)$, $Z(2, -2)$, $Z(2, 2)$, $Z(3, -1)$, $Z(3, 1)$, $Z(4, 0)$, $Z(3, -3)$, $Z(3, 3)$, $Z(4, 2)$, $Z(4, -2)$, $Z(4, 4)$, $Z(4, -4)$. In this paper, we use the definition of the Zernike polynomials as detailed in [2]. The detection bias of all aberrations loaded by the hologram is $\pm 0.5\lambda$ (RMS), and a total of 25 sub-holograms are superimposed (including an imaging hologram). The ratio of light energy on imaging channel to that on holographic image plane is 1:24. The multiplex CGH is computed from the real part of Eq. (6). All the holograms are added and then encoded as a binary phase only hologram. The initial CGH, the coefficient c_i of which is zero, is shown in Fig. 2(a). Because the phase modulation deep of the CGH is π , the light energy of zero diffraction order is zero theoretically. Assuming the hologram is irradiated by the ideal plane wave, the optical field distribution of +1 diffraction order on detection plane is shown in Fig. 2(b). The left half shows the spots on holographic image plane, and the right half shows the spot on focal plane of imaging channel. Because only the light energy of +1 diffraction order is captured by the CCD, an overall +1 order diffraction efficiency is about 50% without considering the little energy of higher diffraction orders. The ratio of light energy on imaging channel to that on holographic image plane is 1:24 and a total of 25 sub-holograms are superimposed, so the diffraction efficiency per beam is about 2%.



Fig. 2. (a) The initial CGH (phase values: black, 0; gray, π) and (b) the optical field distribution on detection plane.

There are 12 pairs of spots on holographic image plane altogether. 24 detection apertures of $1.5\text{mm} \times 1.5\text{mm}$ are selected at the center of each pair of spots on holographic image plane, and the spot energies within the apertures are integrated to calculate the relative light intensity. The diameter of detection aperture is about 4 times the diameter of airy disk. We determine this diameter by considering the light utilization efficiency and response sensitivity. A smaller size of aperture may contribute to a higher response sensitivity, however a lower light utilization effective. Response sensitivity of the aberration can be obtained through simulating the incident light wave with each Zernike-mode aberration to irradiate the hologram and changing the amplitude of that aberration constantly (method 1). Among them, the response sensitivity curve of $Z(2, 2)$, $Z(3, 1)$ are shown in Figs. 3(a) and 3(b). The amplitude of input aberration is taken as abscissa coordinate and the first moment of sensor output signal is taken as vertical coordinate, as P_w in Eq. (4). In the numerical simulation, another calibration method (method 2), with which the coefficient c_i of correction term in CGH is changed constantly, is also used to obtain the response sensitivity. The response sensitivity curve of $Z(2, 2)$, $Z(3, 1)$ are shown in Figs. 3(c) and 3(d) when the coefficient of correction term in CGH is changed. Comparing Figs. 3(a)-3(b) with Figs. 3(c)-3(d), it can be seen that the correction term can compensate wavefront aberration available. In the simulation, we use method 1 to calibrate DHAOS. However, method 2 is a simple and practicable method to a practical system.

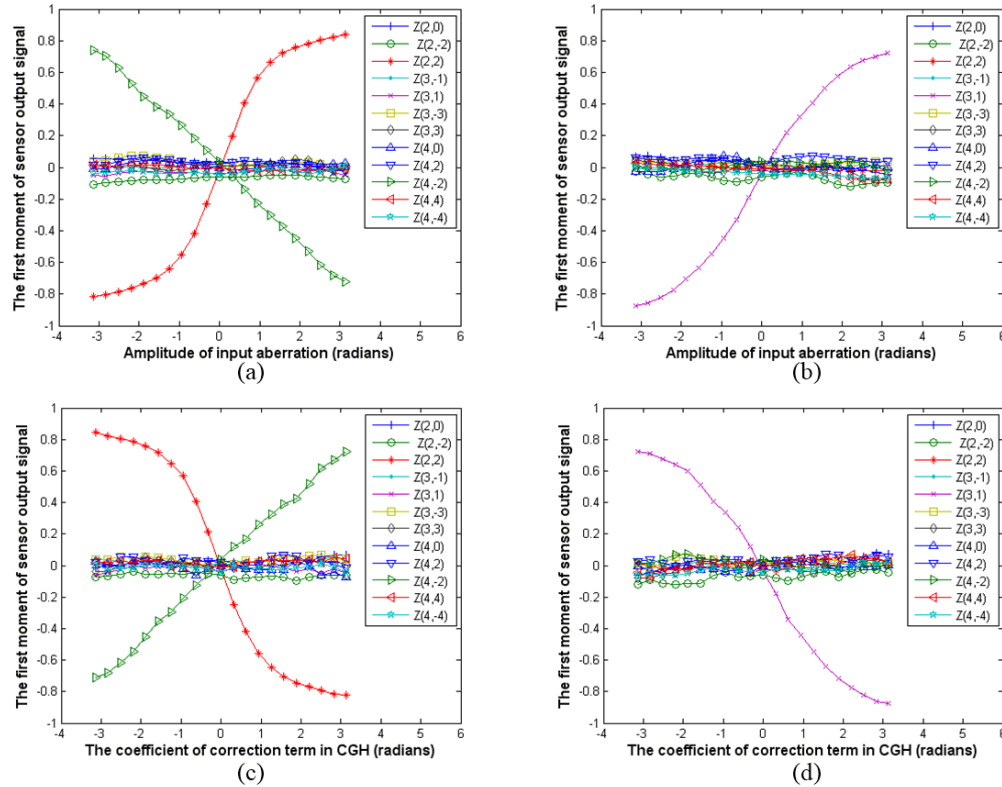


Fig. 3. (a) The sensitivity response curve of $Z(2,2)$ using method 1 to calibrate DHAOS and (b) The sensitivity response curve of $Z(3,1)$ using method 1 to calibrate DHAOS. (c) The sensitivity response curve of $Z(2,2)$ using method 2 to calibrate DHAOS and (d) The sensitivity response curve of $Z(3,1)$ using method 2 to calibrate DHAOS.

As shown in Fig. 3, the response sensitivity curve has good linearity in the case of small aberration. When the aberration coefficient is zero, the slope of curve is defined as the

response sensitivity of this mode aberration. It can be seen from Fig. 3 that this approximation is obviously inaccurate in the case of larger aberrations, and as the aberration increases, the approximation accuracy decreases significantly. However, we believe it will not affect the final closed-loop correction effect in an adaptive optics system because we can detect the “trend” of all mode aberrations and use an iteration method.

It can also be seen from Fig. 3(a) that if incident wavefront is only equipped with aberration of $Z(2,2)$, the sensor not only responds to aberration in this mode, but also to aberration of $Z(4,-2)$, which is the so-called intermodal crosstalk effect of HWFS. Using the method provided by [2] to overcome this effect, an initial calibration is made in the simulation to obtain the response sensitivity matrix S as show in Tab. 1 and the zero point O as show in Tab. 2.

Table 1. Sensitivity Matrix S

		Input aberration mode											
		$Z(2,0)$	$Z(2,-2)$	$Z(2,2)$	$Z(3,-1)$	$Z(3,1)$	$Z(3,-3)$	$Z(3,3)$	$Z(4,0)$	$Z(4,2)$	$Z(4,-2)$	$Z(4,4)$	$Z(4,-4)$
The first moment of sensor output	$P_{Z(2,0)}$	1.56	0.08	0.05	0.00	-0.01	0.00	-0.01	-0.21	-0.36	0.00	0.00	0.02
	$P_{Z(2,-2)}$	-0.02	1.55	-0.02	0.03	0.00	-0.03	0.04	0.05	-0.87	-0.08	-0.10	-0.01
	$P_{Z(2,2)}$	-0.01	0.04	1.63	-0.03	-0.01	0.00	-0.03	-0.01	-0.03	-0.85	0.00	0.03
	$P_{Z(3,-1)}$	-0.04	0.02	-0.01	1.24	0.03	0.00	-0.12	0.00	0.04	-0.03	0.01	0.00
	$P_{Z(3,1)}$	-0.04	-0.01	-0.01	0.01	1.23	0.02	-0.03	-0.05	-0.03	-0.02	-0.04	-0.01
	$P_{Z(3,-3)}$	-0.01	-0.01	-0.02	-0.06	0.41	0.95	0.00	0.12	0.10	0.02	-0.01	-0.02
	$P_{Z(3,3)}$	0.01	-0.02	0.02	-0.42	0.02	0.02	0.95	-0.01	-0.03	0.01	0.02	0.01
	$P_{Z(4,0)}$	-0.23	-0.06	-0.01	-0.02	0.01	0.07	-0.01	1.22	-0.24	-0.03	-0.02	0.03
	$P_{Z(4,2)}$	-0.04	-0.33	-0.01	-0.01	-0.08	-0.05	-0.02	0.03	1.77	-0.06	-0.08	0.01
	$P_{Z(4,-2)}$	0.07	-0.01	-0.55	0.00	0.00	-0.02	-0.01	0.02	-0.04	1.65	-0.02	-0.01
	$P_{Z(4,4)}$	0.21	0.04	-0.05	0.04	-0.02	0.01	0.04	0.04	-0.12	-0.05	0.69	-0.01
	$P_{Z(4,-4)}$	0.01	0.03	0.00	0.01	0.03	-0.01	0.02	0.07	-0.09	0.00	0.01	0.67

Table 2. Zero Point O

		The first moment of sensor output											
		$PZ(2,0)$	$PZ(2,-2)$	$PZ(2,2)$	$PZ(3,-1)$	$PZ(3,1)$	$PZ(3,-3)$	$PZ(3,3)$	$PZ(4,0)$	$PZ(4,2)$	$PZ(4,-2)$	$PZ(4,4)$	$PZ(4,-4)$
Plane wave input		-0.014	0.048	-0.009	-0.042	0.062	-0.037	-0.006	0.033	-0.031	-0.012	0.007	0.026

Aberration Z of various modes can be solved through first moment P_w of output signal of the sensor, as shown in formula.

$$Z = S^{-1} \times (P_w - O) \quad (8)$$

Numerical simulation diagram of DHAOS is shown as the Fig. 4. After loading incident light wave with wavefront aberrations in the simulation, optical field distribution on detection plane is first solved, and then the relative light intensity of each pair of spots on the holographic image plane is calculated to obtain the coefficients of each Zernike-mode aberration, thereby realizing Zernike-mode aberration decomposition of wavefront distortion. Wavefront controller makes PID calculations for each Zernike-mode aberration respectively. Then the coefficient of correction term is changed and a new CGH is generated to correct the wavefront aberration. The optical field distribution of detection plane is solved again, so as to realize closed-loop correction.

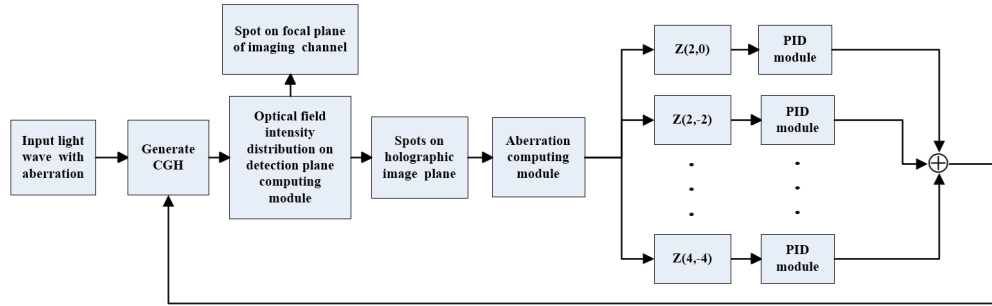
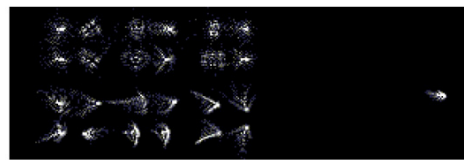
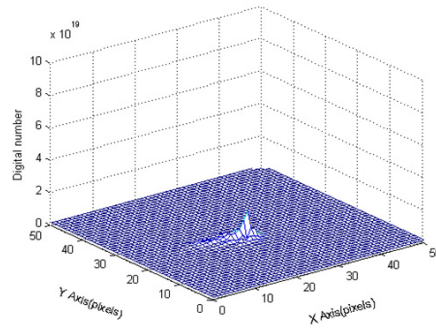


Fig. 4. Numerical simulation diagram of DHAOS.

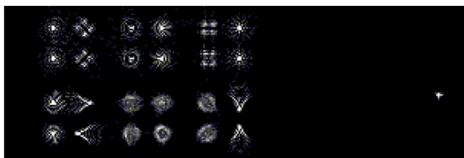
Loading RMS value 0.63λ of wavefront distortion in the simulation ($Z(2, 0)$, $Z(2, -2)$, $Z(3, 1)$, $Z(3, 3)$ are 0.3λ ; $Z(4, 0)$, $Z(4, -2)$, $Z(4, -4)$ are 0.15λ), the spots on the detection plane is shown in Fig. 5(a), and then the intensity distribution of the image spot on the right half detection plane of the system is shown in Fig. 5(b). When the closed-loop adaptive optics system reaches a steady state, the RMS value of the residual aberration is 0.034λ . After final correction, the spots on the detection plane are as Fig. 5(c), and the intensity distribution is shown as Fig. 5(d).



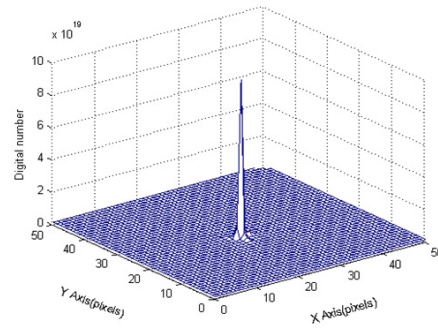
(a)



(b)



(c)



(d)

Fig. 5. Spots on the detection plane (a) before correction, and (c) after final correction. The intensity distributions of the image spot on the right half detection plane (b) before correction, and (d) after final correction.

4. Experiment

We implemented a DHAOS as shown in Fig. 6. This experimental DHAOS uses only one LC-SLM and one CCD sensor. Illumination was provided by an expanded 632.8nm laser

beam. The phase only LC-SLM device (256×256 pixels and $24 \mu\text{m}$ pixel pitch) used here is provided by BNS corporation. LC-SLM has 2π phase modulation depth at the wavelength of 635nm and the diffraction efficiency of the LC-SLM is about 71.5%. The distance between the first image plane and the hologram is 2000mm . The focal length of L2 is 75mm . The distance between the focal spot and the axis is greater than 1cm , and the aberrations of low 8 Zernike-modes are detected, that are $Z(2,0)$, $Z(2,-2)$, $Z(2,2)$, $Z(3,-1)$, $Z(3,1)$, $Z(3,3)$, $Z(3,-3)$, and $Z(4,0)$. The detection bias of all aberrations loaded by the hologram are $\pm 0.25\lambda$ (RMS), and a total of 17 sub-holograms are superimposed (including an imaging hologram). The ratio of light energy on imaging channel to that on HWFS channel is 1:23. A camera with the Truesense Imaging KAI-2093 CCD sensor (1920×1080 pixels and $7.4 \mu\text{m}$ pixel pitch) is provided by Basler corporation to capture the spots at holographic image plane and at imaging channel focal plane. If a CCD with large optical sensor size or butting technique is used, the lens L2 can be removed. An aberrating medium is used to introduce wavefront distortion. DHAOS can detect the tilt/tip aberration of wavefront by way of detecting the centroid of imaging spot. Only the tilt/tip aberration is corrected, all the off-axis aberrations such as coma can be detected accurately in theory. However we do not correct the tilt/tip aberration in this experiment considering that the aberrating medium introduces little tilt /tip aberration.

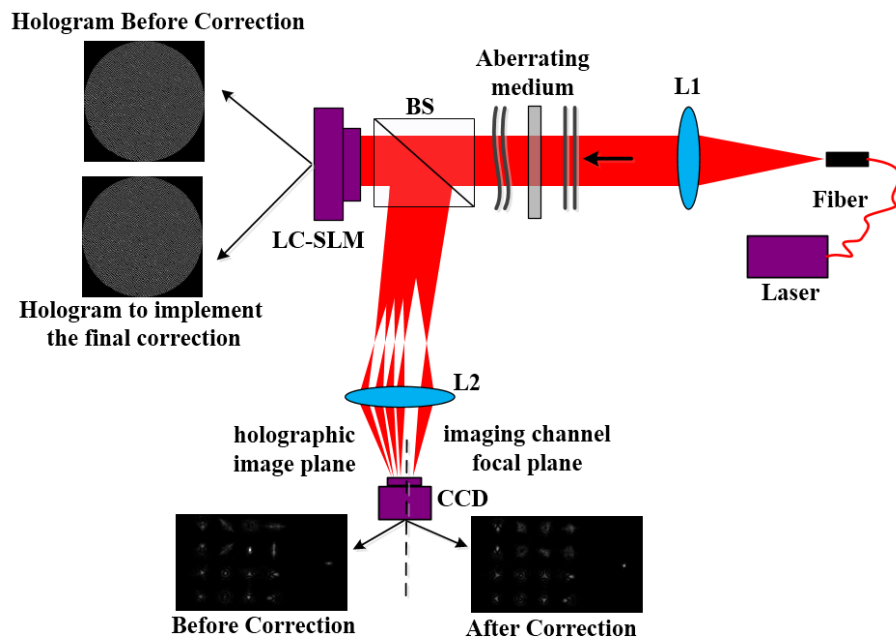


Fig. 6. Experimental configuration of DHAOS.

Before the correction, the CGH on the LC-SLM is shown in Fig. 7(a) and light spots are formed on the CCD as shown in Fig. 7(b), in which the left half shows the spots at holographic image plane, and the right half shows the spot at imaging channel focal plane. The intensity distribution on the right half CCD is shown in Fig. 7(c). The CGH on the LC-SLM to implement the first and final correction are shown in Figs. 7(d) and 7(g). The spots on the CCD plane after the first and final corrections are shown in Figs. 7(e) and 7(h), respectively. The intensity distributions on the right half CCD after the first and final corrections are shown in Figs. 7(f) and 7(m). A video about the variation of spots on CCD plane is also provided, as [Media 1](#).

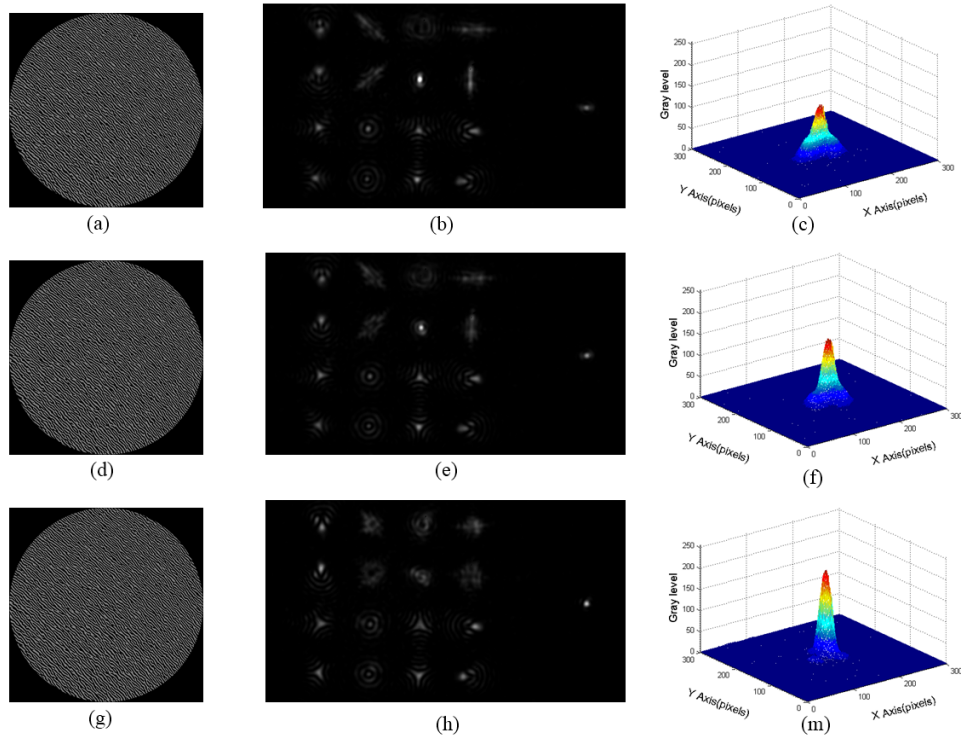


Fig. 7. The CGH loaded on the LC-SLM (a) before correction, (d) to implement the first and (g) final correction (phase values: black, 0; gray, π). Spots on the CCD plane, (b) before correction, (e) after one correction, and (h) after final correction (Media 1). The intensity distributions of the image spot on the right half CCD (c) before correction, (f) after one correction, and (m) after final correction.

Figure 8(a) shows the improvement of Strehl ratio (relative to final frame), calculated from the image spot on the right half CCD, as a function of iteration number. It can be seen that the quality of the image spot on the right half CCD improved considerably as the number of correction cycles increases. Figure 8(b) shows the variation of the RMS of the residual wavefront aberration.

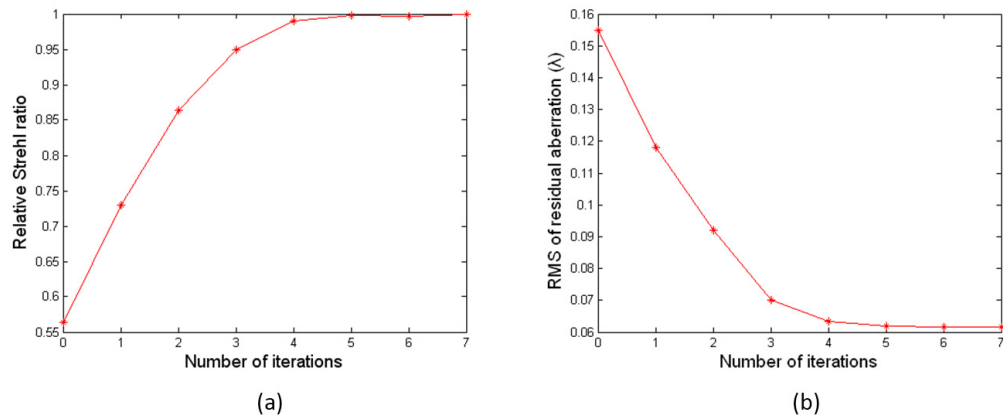


Fig. 8. (a) Improvement in Strehl ratio (relative to final frame) as a function of iterations and (b) RMS value of the residual wavefront aberration as a function of iterations.

5. Discussion and conclusion

In this paper, we proposed a closed-loop adaptive optics system based on dynamic holograms, which implements wavefront sensing and correction simultaneously in a single LC-SLM. Compared with the system proposed in [18], our present proposal can use full LC-SLM and realize higher spatial resolution with less hardware. DHAOS realizes the full capabilities of holographic adaptive optics system via one LC-SLM and one CCD, which is with the same hardware as a single HWFS. DHAOS retains the advantages of HWFS and also has high flexibility of use. The bias of the measured aberration modes loaded on the HWFS can be changed, so that HWFS can keep the highest possible detection accuracy within the most suitable dynamic range. According to the characteristics of multiplexed hologram, the coefficient of imaging hologram, as Λ in Eq. (5), can be adjusted to change the ratio of light energy on imaging channel to that on holographic image plane, enabling more efficient and flexible light use. However we have to point out that DHAOS is only suitable for the applications where the light source is monochromatic in current level of technology. In the future, DHAOS may be applied to the laser beam shaping, retinal imaging, free-space optical communication and astronomical observation based on laser guide star systems.

Acknowledgments

The authors thank Zhaoqi Wang for providing good suggestions. The authors acknowledge helpful suggestions from the reviewers and help from the editors.